Robotics and Computer–Integrated Manufacturing 72 (2021) 102199

Contents lists available at ScienceDirect

Robotics and Computer-Integrated Manufacturing

journal homepage: www.elsevier.com/locate/rcm

Full length article

Impedance controlled human–robot collaborative tooling for edge chamfering and polishing applications

Sreekanth Kana, Srinivasan Lakshminarayanan, Dhanya Menoth Mohan, Domenico Campolo *

School of Mechanical and Aerospace Engineering, Nanyang Technological University, Singapore

ARTICLE INFO

Keywords:
Human Robot Collaboration
Impedance control
Virtual fixtures
Edge chamfering
Edge polishing

ABSTRACT

Surface finishing, as the final stage in the manufacturing pipeline, is a key process in determining the quality and life span of a product. Such a task is characterized by low contact forces and minimal material removal from the object surface. Despite the advancements in machine learning and artificial intelligence, human workforce is still irreplaceable in performing such tasks due to superior dexterity and adaptability, but this is often prone to risks such as hand-arm vibration syndrome due to hand-held tools. Therefore, we propose a collaborative approach to assist the human in carrying out such tasks with the help of two case studies: Human–Robot-Collaborative edge chamfering and polishing tasks, based on an impedance controlled collaborative curve tracing technique.

We propose a collaborative framework, where the robot assists an operator to guide the end-effector/tool along a pre-defined parametric curve. The algorithm is demonstrated in two scenarios. In the first case, we address a collaborative chamfering task whereas the second case focuses on a polishing application (for straight edges). For these kinds of tasks, the curve to be traced assumes the shape of a straight line along the edge. We make use of the compliant feature of a cobot, which allows the user to physically guide the robot in the task space, to generate a mathematical model for the tool path. From the end-user perspective, this is more intuitive than the classical programming-based path planning approaches. In the process of machining, to enhance the path tracking accuracy and to ensure constant tool-surface contact, we implement guidance virtual fixtures through impedance control. As a result, the machining error is reduced.

1. Introduction

Machining processes often leave residual materials on object surfaces, which adversely affects not only the aesthetics but also the performance and life span of the component. Hence, the finishing operations are necessary as the final stage in the manufacturing pipeline where the desired surface profile is achieved through a minimal amount of material removal. Further, key finishing processes such as polishing are considered to be so influential in determining the quality of the final product [1,2] that they can consume up to 50% of total manufacturing time [3–5]. Despite the growth of robotics industry as a whole, the finishing tasks are carried out mainly by skilled labour [6,7] as robots cannot match human performance at contact tooling tasks which involves significant interaction with the dynamic environment [8].

Ideally, in surface tooling, an operator should be effortlessly manoeuvring the tool to modulate process parameters such as the cutting angle and feed rate. Nevertheless, such adjustments are quite challenging in practice, due to the tool weight, inertia and the reaction forces due to cutting. Consequently, the operator is unable to sufficiently control the material removal resulting in variabilities in the manufactured parts. In addition, for typical finishing tasks such as polishing, failing to maintain a constant applied force leads to various surface defects such as form deviations and local imperfections [9]. At the same time, from the operators perspective, maintaining the tool position with a constant force against the chattering and vibrations for prolonged duration leads to ergonomic issues [10].

In the recent past, a new category of robots known as collaborative robots (cobots) has emerged that can share the workplace with humans and interact physically without compromising workplace safety [11,12]. The Human–Robot Collaboration (HRC) can increase productivity as it combines human decision making and adaptability with the precision and repeatability of the robots. Besides, unlike the conventional industrial robots that require expensive work cells, cobots can share the floor with humans leading to lower costs. Such HRC systems are an active research area for a wide range of applications such as surgeries [13,14], drilling and sanding [15], welding [16], and assembly [17,18]. Manufacturing companies, in particular, are increasingly deploying the commercially available cobots such as KUKA iiwa,

* Corresponding author.
E-mail address: d.campolo@ntu.edu.sg (D. Campolo).

https://doi.org/10.1016/j.rcim.2021.102199
Received 27 September 2020; Received in revised form 15 April 2021; Accepted 23 May 2021
Available online 15 June 2021

UR and Franka Panda due to their affordability, safety and intuitive programming capability [8].

Cobots, in comparison to the conventional rigid robots, possess superior design (e.g. backdriveable actuators equipped with force/torque sensors) and control schemes (such as impedance control). According to Hogan [19], a robot is said to be impedance controlled if the force is regulated in response to changes in trajectory, while in admittance control, the robot kinematics is regulated in response to a force. Thus, by regulating the dynamic relationship between the position and force, a robot can deal with unknown environment effectively. For example, Gaz et al. [20] proposed a control algorithm for Human–Robot Collaboration targeting manual polishing process where the workpiece is held by the robot and the tool is carried by the operator. The proposed admittance controller can distinguish between the external force applied by the tool and the force applied due to the human interaction with the robot. As a consequence, the robot can secure workpiece while simultaneously allowing the operator to kinesthetically reorient the robot pose. A similar study on polishing task is presented in [21], demonstrating how the robot can be made to adapt its configuration to account for human ergonomics. The compliance feature of robots is also widely exploited by Learning from Demonstration (LfD) paradigms as outlined in [22], where the robot learns from the human operator by carrying out a collaborative polishing task.

In this paper, we focus on two prominent finishing tasks: *polishing* and *chamfering*. Collaborative surface finishing being an area of active research, several studies have been conducted to bring about the coexistence of humans and robots realizing a shared workspace. For example, the work presented in [23] implements a Human–Robot collaborative platform for surface finishing, particularly targeting polishing tasks. Yet, the human–robot interaction is merely through graphical interfaces and the user is not allowed to enter the workspace while the tool is active. The study discussed in [20] presents a collaborative polishing task, where, the role of the robot is to hold the workpiece while the human carries out the surface tooling. Though the user is free to interact physically with the robot to adjust the pose of the workpiece, the robot does not assist the operator in balancing or manoeuvring of the tool. Peternel et al. [24] proposed a hybrid force/impedance controller, where a collaborative surface polishing task is carried out with an assistive robot. While polishing, the robot ensures proper contact through force control (perpendicular to the surface to be polished) simultaneously allowing a compliant motion in parallel to the surface through impedance control. Furthermore, the robot performs gravity compensation for effortless tool guidance. A similar robot–surface interaction scheme for aircraft canopy polishing is presented in [25]. However, the human does not interact physically with the robot, instead controls it remotely through a joystick to accomplish the task.

Application of an uniform pressure is crucial in obtaining a defect-free polished surface. The work in [26] proposes a collaborative approach which allows the operator to physically guide the robot, simultaneously maintaining the contact between the tool and the surface (thus ensuring a uniform pressure, but normal to the surface).

Collaborative chamfering, however, is a marginally researched area. To the authors' knowledge, no study has been done on the implementation of a human–robot collaborative chamfering task involving user–robot physical interaction. Considering the significance of a quality chamfering for increased product life span and performance, we believe more research needs to be done in this area.

Though Human–Robot Collaborative operations are proven to be very promising to carry out contact tasks, some schemes are necessary to be implemented within an HRC framework to ensure high surface quality and a safe working environment. One of such necessary schemes is the implementation of path/motion constraints to enhance human performance using virtual fixtures [27]. The purpose of virtual fixtures is quite similar to a ruler that is used to draw a straight line, except that the ruler is a tangible fixture. Virtual fixtures are software generated forces used to create the illusion of an actual fixture. They assist the human operators by keeping the tool along the desired path or region and prevent any possible movements towards specific forbidden axis or plane. In collaborative tasks, the virtual fixtures have proven to enhance operator performance by up to 70% [28].

One major advantage of virtual fixtures is that they are not restricted to a specific task and are portable to a wide range of applications as validated by Henry et al. [29]. In fine-manipulation tasks, where the accuracy of task execution is quite crucial and even the smallest of the deviation in the path can drastically affect the completion of a task such as surgery or polishing, such a scheme is indispensable. The majority of the research focusing on the virtual fixtures are developed for teleoperations. Rosenberg studied the implementation and testing of such virtual fixtures for telerobotic manipulation in the peg-hole assembly process with the aid of vision systems [30]. A similar experiment has been performed by Bettini [31], where the target was to achieve two types of motions: manipulator motion (a) towards a point and (b) along a path. As in the previous study, the task is assisted by a vision which delivers the manipulator an idea of the reference path.

In this paper, we extend our previous work on collaborative curve tracing [32] by demonstrating its applicability with the help of actual industrial case studies. Here, we implement virtual fixtures through impedance control to enhance the accuracy of the tooling task, while the proposed curve tracing mechanism generates the tool trajectory in response to the human–robot interaction force. We primarily target tooling tasks such as edge polishing and chamfering (for straight edges), where, one can formulate an analytical model for the tool path. With the proposed approach, an operator physically interacts with a cobot to perform surface machining to achieve the desired profile.

In contrast to the classical programming based path planning approaches, we make use of the geometrical properties of surfaces to identify the tool path along an edge. A cobot with impedance modulation capability can be operated in a compliant (low impedance) mode, where it undergoes a motion in response to external (interaction) forces. Owing to this feature, the operator physically guides the robot in compliant mode to sample triplets of non-collinear points from two intersecting surfaces, to identify the edge to be chamfered/polished. During the execution, to ensure improved path tracking accuracy against lack of hand-arm steadiness and chatter, we implement virtual fixtures through impedance control. Consequently, the chances of tool slipping are averted while operating on unstable regions such as sharp edges, resulting in a safer work environment. Moreover, with the proposed curve tracing technique, the operator is granted fine control over the tool position along the edge (while the robot maintains the user-defined orientation), feed rate and the number of cycles.

In this work, we perform two different trials for each of the tooling tasks, with the robot acting as (a) a gravity compensator and (b) as an assistant, making use of the proposed impedance controlled collaborative framework.

The rest of the paper is organized as follows. In Section 2, we present a theoretical framework for Human–Robot collaborative curve tracing tasks. Sections 3 and 4 demonstrate the applicability of the proposed framework in performing edge chamfering and polishing respectively, followed by the discussion and conclusion in Section 5.

2. Mathematical model for collaborative curve tracing

This section presents a human–robot collaborative scheme for curve tracing tasks following our previous work presented in [32].

2.1. Theoretical background

2.1.1. Kinematics of 3D curve

In many of the industrial edge finishing tasks, especially where the object's shape is a geometric primitive, one can express the tool

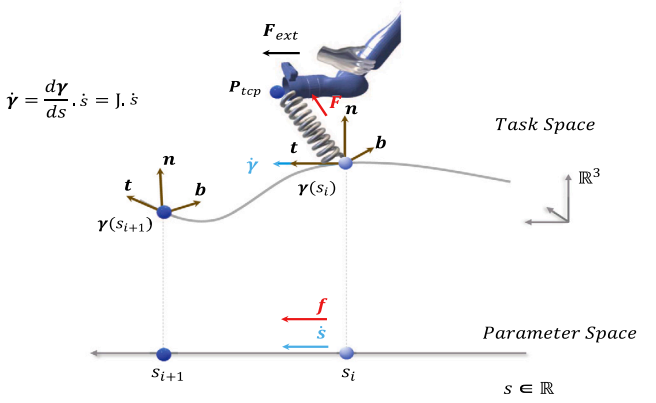

Fig. 1. Motion of the tool frame along a 3D parametric reference trajectory under an applied user force.

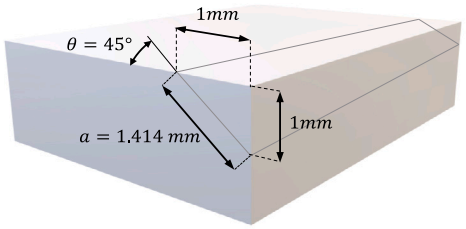

Fig. 2. Desired chamfer with a 45 degrees bevel and 1.414 mm setback.

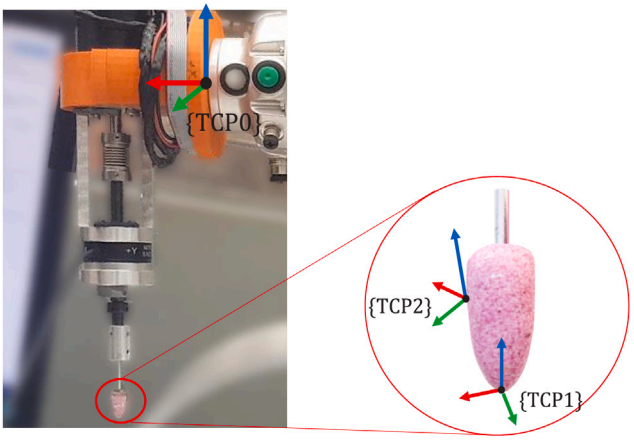

Fig. 3. Two TCPs defined on the tool with respect to the TCP0 to (a) sample the surface points (TCP1) and (b) to perform the tooling task (TCP2).

trajectory in a parametric fashion. Such a trajectory can be generalized in 3D space as

$$\boldsymbol{\gamma}(s) : \mathbb{S} \longrightarrow \mathbb{R}^3, \tag{1}$$

where $s \in \mathbb{S} \subset \mathbb{R}$ is a real parameter. For a given value of the parameter s, the corresponding 3D point $\boldsymbol{\gamma}(s)$ is bound to stay on the curve, as shown in Fig. 1.

As the parameter s changes with time t, its time derivative $\dot{s} := \frac{ds}{dt}$ will induce a velocity $\dot{\boldsymbol{\gamma}}$

$$\dot{\boldsymbol{\gamma}} = \frac{d\boldsymbol{\gamma}}{ds}\dot{s} = \boldsymbol{\gamma}'\,\dot{s} \tag{2}$$

Note that the 'dot'() derivative is with respect to time and the 'prime' derivative (′) is with respect to the parameter s.

Eq. (2) maps velocity in the parameter space into velocities in 3D space, defining thus the *Jacobian*:

$$J := \boldsymbol{\gamma}' \tag{3}$$

The velocity $\dot{\boldsymbol{\gamma}}$ is always tangent to the curve and the tangent unit vector can be defined as

$$\boldsymbol{t} := \frac{\boldsymbol{\gamma}'}{|\boldsymbol{\gamma}'|}, \tag{4}$$

where,

$$|\boldsymbol{\gamma}'| := \sqrt{\boldsymbol{\gamma}' \circ \boldsymbol{\gamma}'} \tag{5}$$

and $\circ$ is the dot-product in 3D space ($\boldsymbol{a} \circ \boldsymbol{b} = \boldsymbol{a}^T\boldsymbol{b}$, for any $\boldsymbol{a}, \boldsymbol{b} \in \mathbb{R}^3$) [33], *unit bi-normal* ($\boldsymbol{b}$), and *unit normal* ($\boldsymbol{n}$) vectors can be defined respectively as

$$\boldsymbol{b}(s) := \frac{\boldsymbol{\gamma}' \times \boldsymbol{\gamma}''}{|\boldsymbol{\gamma}' \times \boldsymbol{\gamma}''|}, \qquad \boldsymbol{n}(s) := \boldsymbol{b} \times \boldsymbol{t}, \tag{6}$$

where, $\times$ represents the vector product in $\mathbb{R}^3$.

The tangent, normal and bi-normal vectors form a so called *moving frame* whose orientation with respect to the robot base frame is captured by the following orientation matrix.

$$\boldsymbol{R}(s) = [\boldsymbol{t}(s)\ \boldsymbol{n}(s)\ \boldsymbol{b}(s)] \tag{7}$$

The complete description of the moving frame, including origin and orientation along the 3D curve, is encoded by a 4×4 matrix as below:

$$G(s) = \begin{bmatrix} \boldsymbol{t}(s) & \boldsymbol{n}(s) & \boldsymbol{b}(s) & \boldsymbol{\gamma}(s) \\ 0 & 0 & 0 & 1 \end{bmatrix} \tag{8}$$

As the parameter s changes in time, the matrix $G(s)$ in (8) defines a frame sliding along the curve $\boldsymbol{\gamma}(s)$, which serves as the desired end-effector/tool frame for the robot.

2.1.2. Dynamics of curve tracing

For the collaborative tooling tasks in this paper, we employ an impedance control based approach. This enables us to modulate the stiffness values to achieve compliance in the desired directions simultaneously restricting undesirable motions.

For a robot manipulator, the joint space dynamics can be expressed in the form [34,35]

$$M(\boldsymbol{q})\ddot{\boldsymbol{q}} + C(\boldsymbol{q}, \dot{\boldsymbol{q}})\dot{\boldsymbol{q}} + \boldsymbol{g}(\boldsymbol{q}) = \boldsymbol{\tau}_c + J^T\boldsymbol{F}_{ext}, \tag{9}$$

where, $\boldsymbol{q} \in \mathbb{R}^n$ is the vector of joint angles, $M(\boldsymbol{q}), C(\boldsymbol{q}, \dot{\boldsymbol{q}}) \in \mathbb{R}^{n\times n}$ are the inertia and Coriolis matrices respectively, $\boldsymbol{g}(\boldsymbol{q})$ is the gravitational torque, $\boldsymbol{\tau}_c$ is the control torque, and $J^T\boldsymbol{F}_{ext}$ is the joint torque vector generated by an externally applied force (under a collaborative operation, $\boldsymbol{F}_{ext}$ is generated from the human–robot physical interaction).

To implement impedance control for the collaborative curve tracing, the robot dynamics is better expressed in the Cartesian coordinate frame as given below.

$$\Lambda(\boldsymbol{q})\ddot{\boldsymbol{x}} + \mu(\boldsymbol{q}, \dot{\boldsymbol{q}})\dot{\boldsymbol{x}} = \boldsymbol{F} + \boldsymbol{F}_{ext}, \tag{10}$$

where, $\boldsymbol{x} \in \mathbb{R}^3$ is the Cartesian position of the tool/end-effector, $\Lambda(\boldsymbol{q}) \in \mathbb{R}^{3\times3}$ is the end-effector inertia matrix, $\mu(\boldsymbol{q}, \dot{\boldsymbol{q}})$ is the Coriolis matrix, and $\boldsymbol{F}$ is a Cartesian control force (to be defined later on) which determines the control torques according to $\boldsymbol{\tau}_c = \boldsymbol{g}(\boldsymbol{q}) + J^T\boldsymbol{F}$.

Compliant manipulators such as the KUKA iiwa can operate both in *impedance mode* (where, the user is free to modulate the stiffness values to perform impedance control) and *rigid mode* (where, the user

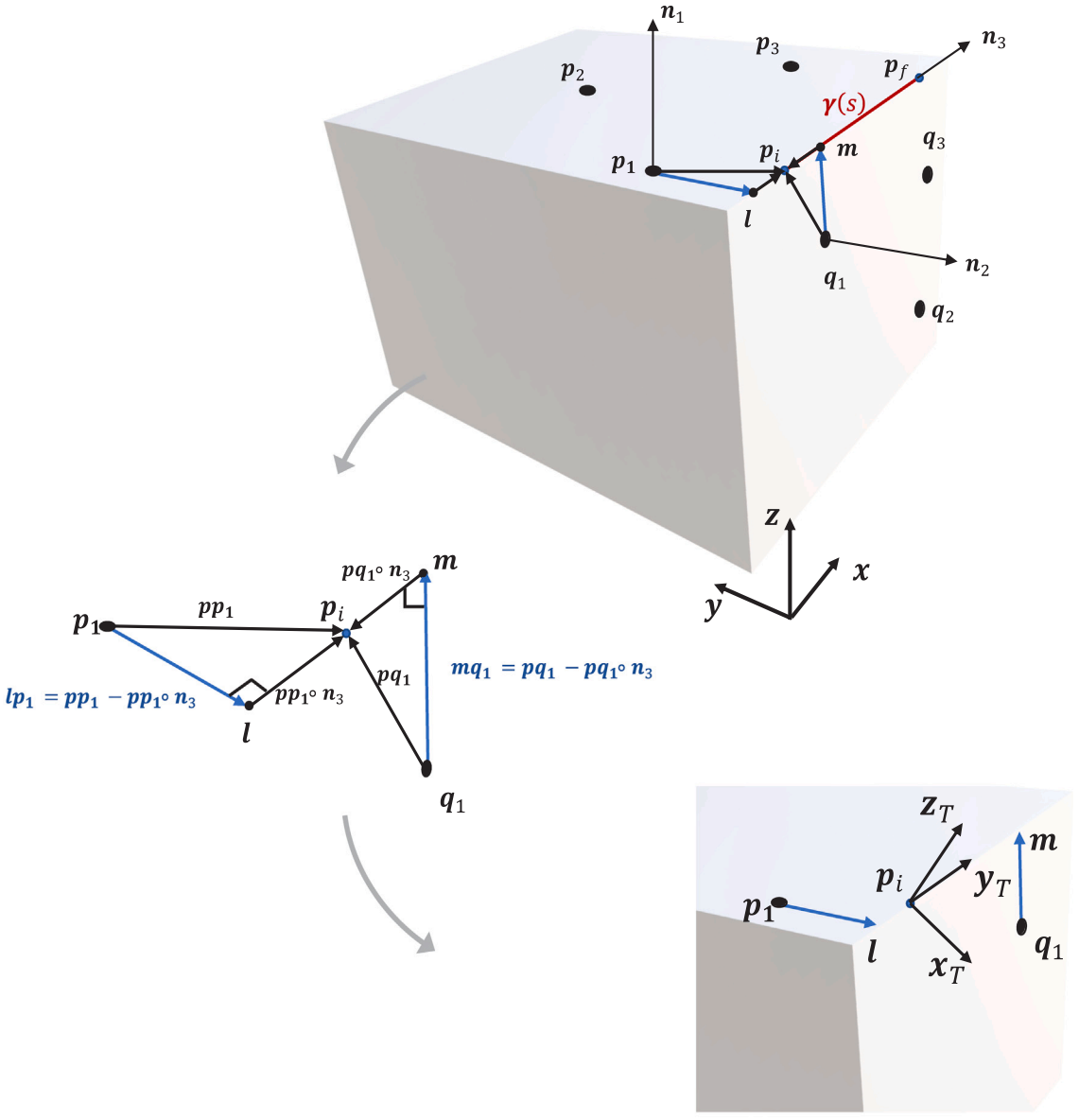

Fig. 4. Defining the tool frame (TCP2) orientation, based on the sampled surface points $(\boldsymbol{p}_1, \boldsymbol{p}_2, \boldsymbol{p}_3)$ and $(\boldsymbol{q}_1, \boldsymbol{q}_2, \boldsymbol{q}_3)$.

has no control over the stiffness values, which are internally set to realize a rigid behaviour). In the impedance mode, two main frames are of concern: the virtual frame (also know as the *setpoint*), defined by the user, and TCP (Tool Center Point) frame, representing the actual pose of the robot. A virtual, generalized spring can be imposed with linear stiffness parameters as illustrated in Fig. 1. Such a spring imposes a force (according to a generalized Hooke's law) on TCP such that the TCP frame is attracted towards the virtual frame.

The virtual frame can be seen as an *equilibrium* for the TCP frame. For any value of the parameter s, the matrix $G(s)$ in (8) can be used to define a virtual frame bound to stay on the curve and to be aligned with it (i.e. one axis of the virtual frame is always aligned with the tangent $\boldsymbol{t}$ to the curve, the remaining two axes with $\boldsymbol{n}$ and $\boldsymbol{b}$, respectively). For collaborative operations, along a curve, we would like the operator to be able to easily push the KUKA robot (or better, its TCP frame) along the curve but not away from it. This can be achieved by imposing high stiffness in direction perpendicular to the curve and low stiffness along the curve and by allowing the virtual frame to *slide* on the curve itself. Similarly to a bead in a wire, the bead should only move if pushed along the wire, but not if pulled away from it. In other words, the bead is only sensitive to forces acting along the wires, i.e. to their *projection* along the tangent $\boldsymbol{t}$ to the wire. To determine the dynamics of the bead (origin of the virtual frame) in a wire, we can assume that the bead is subjected to a control force (note that here we only consider the translational motion for discussion) due to a generalized spring and damper coupling between the bead itself and the origin of the TCP frame $\boldsymbol{P}_{tcp}$.

$$\boldsymbol{F} = K\Delta\boldsymbol{x} + D\Delta\dot{\boldsymbol{x}} \qquad \text{where } \Delta\boldsymbol{x} := \boldsymbol{P}_{tcp} - \boldsymbol{\gamma}(s) \tag{11}$$

$K, D \in \mathbb{R}^{3\times3}$ are the stiffness and the damping matrices respectively. In this paper, we are mostly concerned with the stiffness matrix, while the damping matrix will be use for stabilization purposes and is often set to be proportional to the stiffness matrix [36].

A linear stiffness matrix is the Hessian (i.e. second derivative) of an elastic function and, as such, it is represented by a symmetric matrix which can always be factored in a diagonal form

$$K = \begin{bmatrix} k_x & 0 & 0 \\ 0 & k_y & 0 \\ 0 & 0 & k_z \end{bmatrix}, \tag{12}$$

where, k_x, k_y, k_z are the eigenvalues of the stiffness ellipsoid. In this paper, we shall simply consider principal axes for the stiffness ellipsoid

which lie along the x, y and the z directions of the TCP frame. In the scenario of interest in this work, the tool compliance can simply be set by maintaining constant stiffness eigenvalues and by modulating the TCP orientation in accordance with the workpiece geometry. In this work, we only modulate the stiffness but not the damping values. Hence matrix D remains constant.

Eq. (11) is designed to set a given point $\gamma(s)$, on the curve, as an equilibrium point for the robot TCP. The means that without human intervention (i.e. $F_{ext} = 0$ in (9) or (10)), the robot TCP is expected to coincide with $\gamma(s)$. However, to allow for the point $\gamma(s)$ to actually 'slide' along the curve, the parameter s has to be updated. One simple way to do so, is to induce a rate of change $\dot{s}$ for the parameter proportional to the amount of force along the curve, i.e. $F \circ \gamma'$, i.e.

$$\dot{s} = \alpha(F \circ \gamma'), \tag{13}$$

where α is a damping parameter. Considering a time-discretization with time sample $s_1, s_2, \dots s_i$, the dynamics can be written as an update equation

$$s_{i+1} = s_i + \Delta t(\alpha(F \circ \gamma')), \tag{14}$$

where, Δt is the sampling time. In the subsequent sections, we show the applicability of this collaborative curve tracing technique in the context of typical chamfering and polishing (for a straight edges) tasks, where, one can express the tool path analytically.

3. Experimental case study 1: Edge chamfering

In this section, we test and validate the proposed approach for a collaborative chamfering application, where the goal is to achieve a chamfer with a 45 degrees bevel with 1.414 mm setback as illustrated in Fig. 2.

In this work, we assume that all the edges to be machined are straight edges formed by the intersection of two adjacent planes. However, this can be extended to more general surfaces as discussed in Section 5.

The collaborative chamfering is carried out in two phases. In the first phase, we identify the edge to be chamfered and formulate an analytical expression for the tool path. The second phase focuses on the collaborative chamfering by modulating the impedance parameters of the robot with respect to the generated path. The impedance is set in such a way that the operator is able to effortlessly guide the tool along the edge to be chamfered, simultaneously averting the chances of the tool motion/slipping in orthogonal directions.

To generate a tool trajectory along the edge, we derive a mathematical expression for the moving (tool) frame along the edge. The impedance parameters will subsequently be set with reference to this frame to enable collaborative execution of the task. Since an edge is nothing but the line of intersection between its adjacent face planes, the problem can now be reduced into obtaining the expression for the face planes characterizing the edge.

As a plane can mathematically be expressed with a set of three non-collinear points on its surface, by sampling two such triplets (manually guiding the robot in compliance mode) from each of the intersecting surfaces, the edge can be determined. At this stage, it is imperative that we define two different TCPs for each of the two phases. This is because the points on the surface are best sampled with the tip of the tool whereas, during tooling, it is the periphery of the tool that makes the contact with the edge. To that end, two TCP frames, one at the tool-tip (TCP1), to sample the points from the surface and the other (TCP2) on the tool periphery (which is basically the tool contact point with the edge during chamfering) are defined as shown in Fig. 3. The tool used here is a conical shaped grinding head, on which the frames are defined with reference to the robot flange frame (TCP0). To calibrate the position of the TCP1 and TCP2 coordinate systems, we use the *xyz 4-point method* available in the KUKA controller. While the orientation of TCP1 is maintained as the same as that of the flange, TCP2 orientation is identified based on the chamfer criteria (45 degrees with respect to the edge in this particular case) as discussed in the next section.

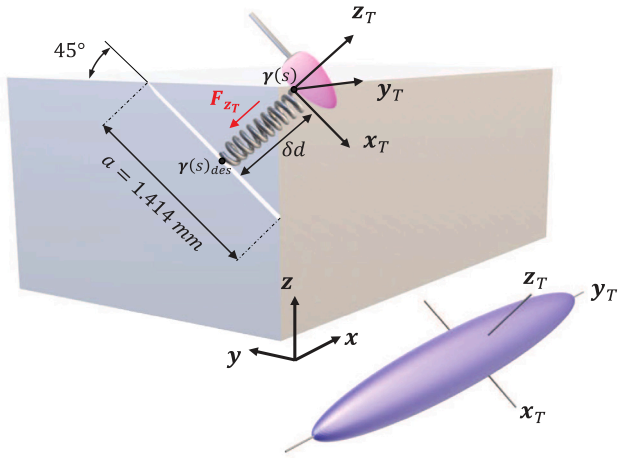

Fig. 5. An energy ellipsoid defines the compliance along the axes of the tool frame TCP2. For a given applied energy, one can achieve more displacement along the edge, but restricted motion in the orthogonal directions.

3.1. Edge identification and tool kinematics

If S_1 and S_2 are the adjacent faces to the edge of interest and (p_1, p_2, p_3), (q_1, q_2, q_3) are respectively the sets of sampled (in such a way that the distance between each other is maximized) points (Fig. 4), then the unit normals to the surfaces can be obtained respectively as

$$n_1 = \frac{(p_3 - p_1) \times (p_2 - p_1)}{|(p_3 - p_1) \times (p_2 - p_1)|} \tag{15}$$

$$n_2 = \frac{(q_3 - q_1) \times (q_2 - q_1)}{|(q_3 - q_1) \times (q_2 - q_1)|} \tag{16}$$

The unit vector directing along the edge is computed as follows:

$$n_3 = n_1 \times n_2 \tag{17}$$

To define the boundary points (p_{ini} and p_{fin}) for the tool path, a set of linear equations are considered as given below:

$$(p_{ini} - p_1) \circ n_1 = 0$$
$$(p_{ini} - q_1) \circ n_2 = 0$$
$$p_{ini} \circ n_3 = min((p_i \circ n_3), (q_i \circ n_3))$$
$$(p_{fin} - p_3) \circ n_1 = 0$$
$$(p_{fin} - q_3) \circ n_2 = 0$$
$$p_{fin} \circ n_3 = max((p_i \circ n_3), (q_i \circ n_3))$$

Hence the trajectory of the moving frame (TCP2 frame) along the edge can be parameterized as

$$\gamma(s) = p_{ini} + (p_{fin} - p_{ini})s, \tag{18}$$

where, $0 \le s \le 1$.

To identify the orientation of the TCP2 frame, we have to take the chamfer requirements into account (Fig. 2).

Having decided the chamfer requirement, the next step is to define the orientation for TCP2 such that the tool is always oriented at angle of 45 degrees with respect to the edge. With reference to Fig. 4, such a frame centered at p_{ini} can be formulated as follows:

$$z_T = \frac{lp_1 + mq_1}{|lp_1 + mq_1|} \qquad y_T = n_3 \qquad x_T = y_T \times z_T \tag{19}$$

Hence, a moving frame along the tool path at any instant can be represented using Eq. (8).

$$G(s) = \begin{bmatrix} x_T & y_T & z_T & \gamma(s) \\ 0 & 0 & 0 & 1 \end{bmatrix} \tag{20}$$

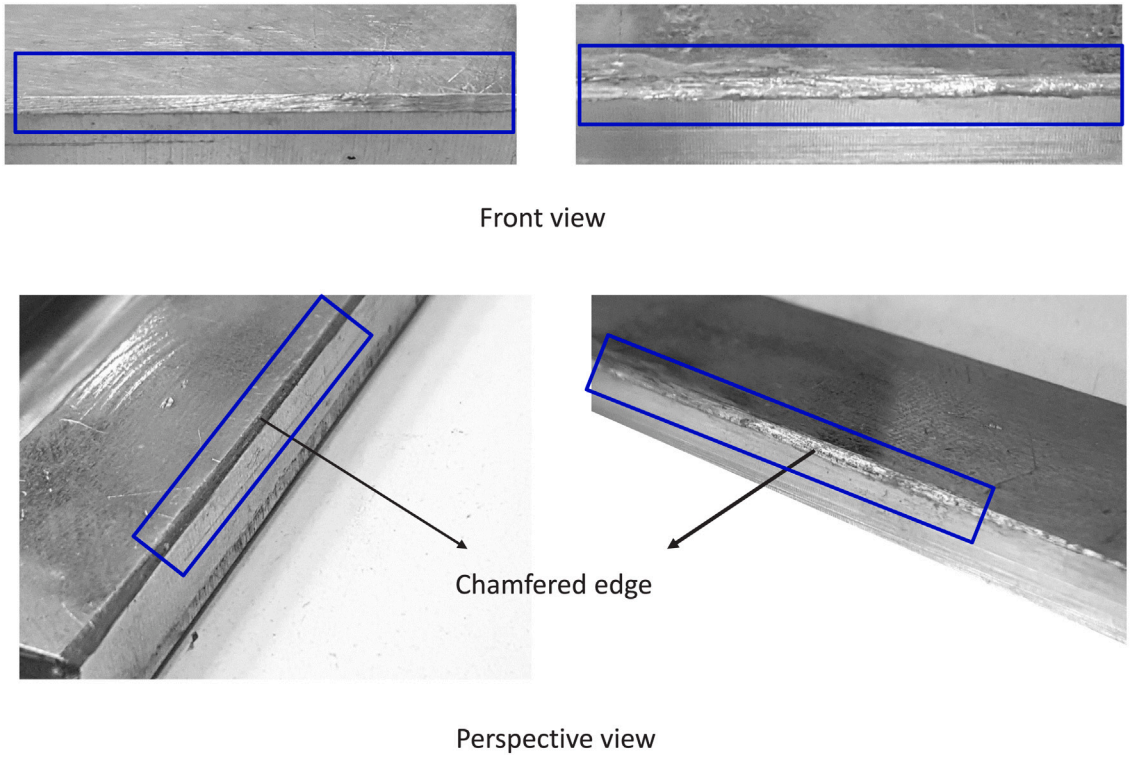

Fig. 6. Qualitative analysis of the resulting chamfer quality (a) with impedance controlled curve tracing (left) and (b) without impedance controlled curve tracing (right).

3.2. Tool dynamics

For describing the tool dynamics, first we make an assumption on the rigidity of the workpiece material. In this study, we focus on objects with uniform rigidity. In other words, the object offers the same amount of resistance to the material removal throughout the machining process. We apply a machining force $\boldsymbol{F}_z$ (decreasing towards the target (chamfer) surface) along the $\boldsymbol{z}_T$ direction through impedance control as

$$\boldsymbol{F}_{z_T} = -k_{z_T}\delta d\,\boldsymbol{z}_T, \tag{21}$$

where, δd is the offset ($\frac{a}{\sqrt{2}}$ in this specific case (Fig. 5)) along $\boldsymbol{z}_T$ and k_{z_T} is the stiffness in the direction of $\boldsymbol{z}_T$ and is obtained as

$$k_{z_T} = \frac{|\boldsymbol{F}_{z_T}|}{\delta d} \tag{22}$$

To realize this force, the desired TCP2 frame is modified to be the following:

$$G(s) = \begin{bmatrix} \boldsymbol{x}_T & \boldsymbol{y}_T & \boldsymbol{z}_T & \boldsymbol{\gamma}(s)_{des} \\ 0 & 0 & 0 & 1 \end{bmatrix} \tag{23}$$

where, $\boldsymbol{\gamma}(s)_{des} = \boldsymbol{\gamma}(s) + \begin{bmatrix} a\boldsymbol{x} \\ 0 \\ -a\boldsymbol{z} \end{bmatrix}$.

Here, the elastic properties of the stiffness matrix K (Eq. (12)) can be described by an energy ellipsoid (Fig. 5) as

$$\Delta\boldsymbol{x}^T K \Delta\boldsymbol{x} = 2\epsilon, \tag{24}$$

where, $\Delta\boldsymbol{x} \in \mathbb{R}^{3\times1}$ is the elastic displacement in a generic direction in response to a constant applied energy ϵ. For collaborative tooling, the given stiffness setting allows smooth guidance along the edge but minimal movements in orthogonal directions.

For objects with non-uniform rigidity, a force adaptation approach can be integrated $\boldsymbol{F}_{z_T}$ to ensure material removal (See Section 5).

3.3. Collaborative task execution

3.3.1. Experimental setup

The workpiece used for the experiment was an aluminium block of dimensions of 15 cm × 7 cm × 7 cm. A Dremel with an attached conical grinding head was mounted on the end-effector of a KUKA iiwa.

Step: 1: *Sampling the points from the adjacent faces*

To identify the normals to each of the intersecting faces, the operator physically guided the robot and sampled 3 non-collinear points from each of the surfaces. Here, the robot operates in compliant mode with very low stiffness ($k_x = k_y = k_z = 500$ N/m) for each of the Cartesian degrees of freedom (with respect to the robot base frame)

Step 2: *Collaborative chamfering*

The chamfering was performed under two different impedance settings based on the role of the robot in the collaborative operation:

(a) Without impedance controlled curve tracing

In this trial, the role of the robot is to assist the human in balancing the tool weight (similar to a gravity compensator). The Cartesian stiffness values for both the translational and the rotational motions were set to low ($k_x = k_y = k_z = 500$ N/m and $k_\alpha = k_\beta = k_\gamma = 300$ Nm/rad respectively) to enable tool motion predominantly controlled by the user. Note that the chamfer parameters are monitored solely by the operator and the quality of the resulting chamfer depends on the skill of the operator alone.

(b) With impedance controlled curve tracing.

In this mode, we impose constrains on the human–robot motion (through impedance control) to achieve higher path accuracy, granting the operator control over parameters such as the cycle time and the number of cycles.

For the chamfering task, to enable compliance along the edge, the virtual stiffness in the direction of the edge ($\boldsymbol{y}_T$) is set to a low value ($k_{y_T} = 800$ N/m) whereas the stiffness along $\boldsymbol{x}_T$ is set to be high ($k_{x_T} = 3000$ N/m). The required setback of 1.414 mm with a bevel of

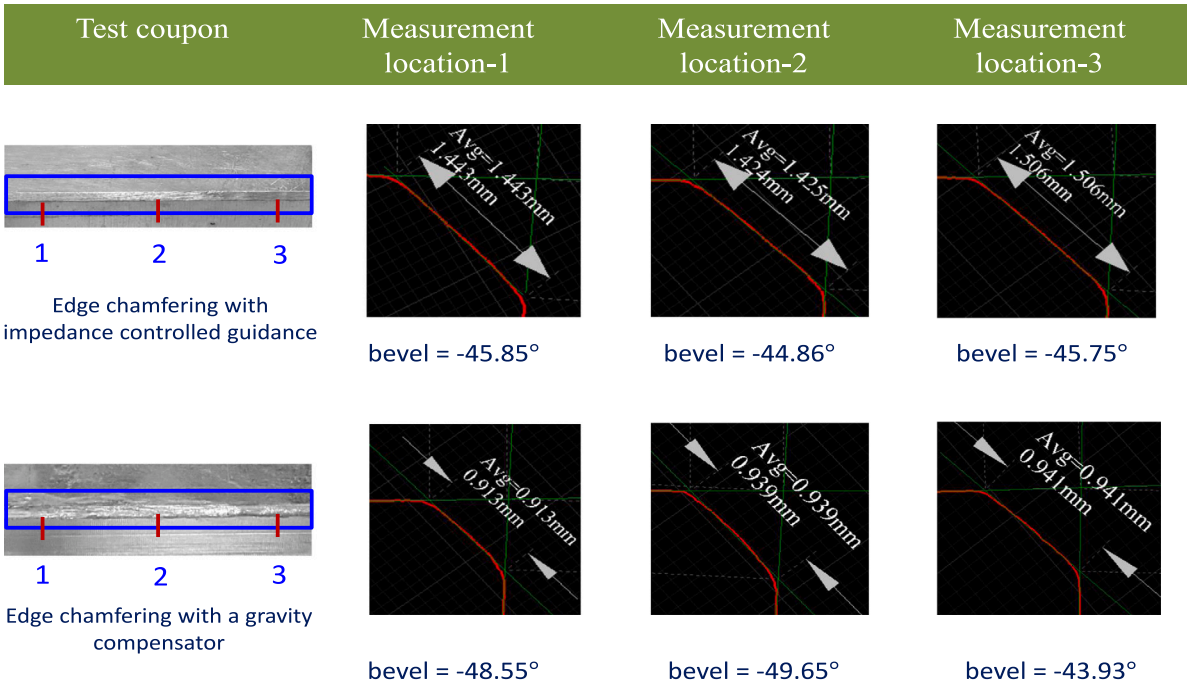

Fig. 7. To compare the results obtained from the impedance-controlled curve tracing and the gravity compensator modes, measurements were taken using a GapGun device at three different locations defined by the user. For a desired bevel of 45 degrees and setback of 1.414 mm, the proposed approach yielded a more accurate result at all three locations. At each location, the GapGun device takes a set of measurements and outputs both the instantaneous and the average measurements, as indicated in the images.

45 degrees calculates the value of δd as 0.707 mm. To achieve a desired force ($\boldsymbol{F}_{z_T}$) of 2 N the stiffness k_{z_T} is set to be 2828 N/m.

Once the sampling is done the robot detects the edge and moves to the initial point (where, the commanded TCP1 position is $\boldsymbol{\gamma}(0) - \delta d \boldsymbol{z}_T$ and its expected position is $\boldsymbol{\gamma}(0)$, thus getting pulled towards destination point with a force $\boldsymbol{F}_{z_T}$) of the trajectory. Subsequently, the operator guides the robot along the edge to perform the chamfering and this is continued until the final chamfer surface (where, $\delta d \to 0$) is achieved.

3.3.2. Results and analysis

In the first phase, we used the user sampled points to identify the line of intersection of the faces sharing the edge of interest. After phase two, in which the trial was conducted with two distinct modes of impedance setting, the resulting chamfered surfaces are shown in Fig. 6.

From visual inspection, it can be seen that with impedance controlled guidance, despite the trial was performed by an unskilled operator, the resulting surface appeared to have lesser defects and more consistency compared to the one where, the robot was acting as a simple gravity compensator. The resulting chamfer surface dimensions, for both the modes of operation, have been measured with a GapGun (which is a laser measuring tool) at three user-defined locations (Fig. 7).

4. Experimental case study 2: Edge polishing

The second set of trials with the proposed framework was conducted on an edge polishing task for an Aluminium workpiece. As in the previous section, the process can be divided into two phases. In the first phase, the edge identification is facilitated by the 6-points sampling method detailed for the edge chamfering process. Here, the tool used is a polishing pad and just a single TCP is sufficient both for sampling and tooling as shown in Fig. 8.

In the second phase, the operator performs collaborative polishing with the robot operating in (a) gravity compensator mode and (b) impedance controlled guided mode respectively (see Fig. 9).

4.1. Tool kinematics

With reference to Fig. 4, the parametric expression for the edge can again be defined as:

$$\boldsymbol{\gamma}(s) = \boldsymbol{p}_{ini} + (\boldsymbol{p}_{fin} - \boldsymbol{p}_{ini})s, \tag{25}$$

where, $0 \leq s \leq 1$.

$$\boldsymbol{z}_T = -\boldsymbol{n}_2 \qquad \boldsymbol{y}_T = \boldsymbol{n}_3 \qquad \boldsymbol{x}_T = \boldsymbol{y}_T \times \boldsymbol{z}_T \tag{26}$$

With reference to Fig. 10, if the polishing tool radius is denoted as r, then its pose at any instant can be expressed by the following homogeneous matrix:

$$G(s) = \begin{bmatrix} \boldsymbol{x}_T & \boldsymbol{y}_T & \boldsymbol{z}_T & \boldsymbol{\gamma}(s) - r\boldsymbol{z} \\ 0 & 0 & 0 & 1 \end{bmatrix} \tag{27}$$

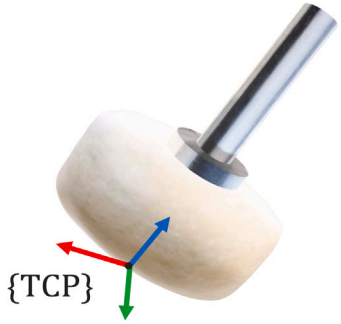

Fig. 8. Tool TCP defined on a polish pad for edge polishing.

4.2. Collaborative execution

4.2.1. Experimental setup

The workpiece for the experiment was an aluminium block. A Dremel with an attached polishing tool with a diameter of 8 mm was mounted on the end-effector of the KUKA iiwa.

Step 1: *Sampling the points from the adjacent faces* (see 3.3.1)

Step 2: *Collaborative polishing*

We conducted two sets of trials under two different impedance settings based on the role of the robot in the collaborative operation:

(a) Without impedance controlled curve tracing (see 3.3.1)

(b) With impedance controlled curve tracing.

In this mode, the robot imposes constraints (through impedance control) on the human motion thus allowing the operator to have control over the process parameters such as the cycle time and the number of cycles without compromising the path accuracy.

To allow compliant motion along the edge, the virtual stiffness in the direction of the edge ($\boldsymbol{y}_T$) is set to a very low value (k_{y_T} = 800 N/m) whereas the stiffness values along $\boldsymbol{x}_T$ and $\boldsymbol{z}_T$ is set to be high ($k_{x_T} = k_{z_T} = 3000$ N/m) to avoid possible tool slipping.

4.2.2. Results and analysis

The resulting polished surfaces after the two sets of trials are shown in Fig. 11. From the figure, it is evident that the quality of the polished surface is inferior when the robot acted as just a gravity compensator (i.e. without impedance controlled guidance). On the other hand, when the impedance control is used to impose motion constraints on the

Fig. 9. Example of a human–robot collaborative edge polishing application, where the human physically interacts with the robot to accomplish the task.

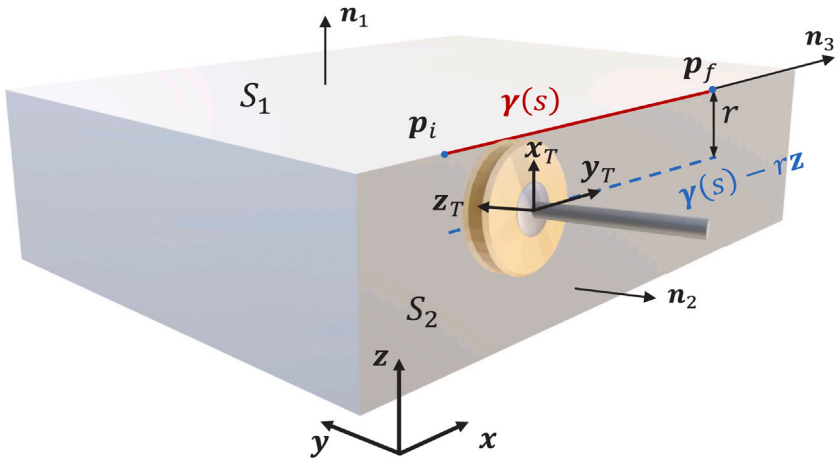

Fig. 10. The tool orientation is defined in such a way that the force is applied perpendicular to the surface while the tool traverse the trajectory $\gamma(s) - rz$.

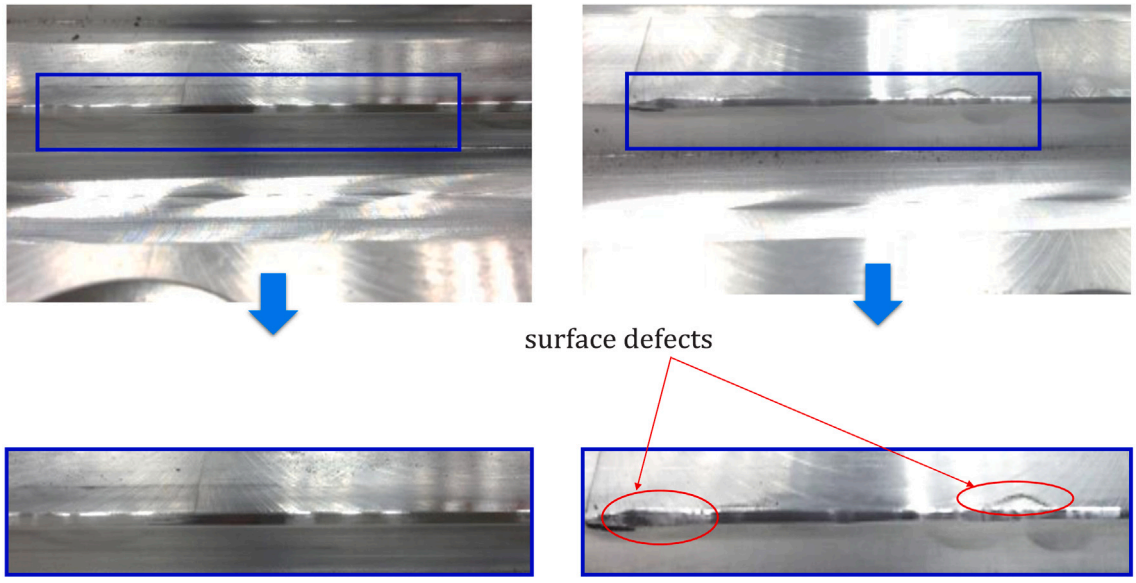

Fig. 11. Qualitative analysis of the polished surface with (a) impedance controlled curve tracing (left) (b) the robot acting as a gravity compensator (right). With the proposed approach the defects present in the gravity compensation mode are subdued.

human–robot motion, the quality is found to be superior in comparison. In addition, the operator asserted that when the impedance control based guidance was employed, it was relatively easy for him to guide the tool along the edge as the vibrations due to the tool-surface contact and the lack of hand-arm steadiness were curtailed.

5. Discussion and conclusion

In contrast to the conventional methodologies for tool path generation involving teach pendants and intensive coding, one can take advantage of the geometrical features of objects to identify the desired tool path. The assistance of a compliant robot renders this easier by enabling the operator to physically guide the tool across the workspace to sample key surface points, thereby obtaining a mathematical representation for the tool trajectory. This is observed to be relatively faster and less tedious even for a novice operator. Analysing the experimental results of both chamfering and polishing tasks, we observed that, with a gravity compensator alone, the novice operator is unable to accurately achieve the desired surface profile. As an outcome of our work, we show that the proposed impedance controlled approach enhances product quality.

The proposed approach is built upon two key assumptions. Our primary assumption considers all edges to be machined as straight edges which can be represented in a parametric fashion. Although our approach is limited to straight edges, it can be generalized to free-form surfaces by integrating the trajectory generation techniques presented in [37], which will be the course of action for our future work.

Another major assumption is that the object surface possesses uniform rigidity, which does not hold for all the materials. Therefore, the force of interaction as given in Eq. (22) (which gradually reduces as the tool approach the target surface profile) might not be ideal for surfaces with increasing hardness. To surpass this shortcoming, we aim to integrate an adaptation algorithm [38], which not only modulates the force of interaction to account for different stiffness properties but also carries out machining without the knowledge of the required force. The fact that this algorithm is implemented through impedance control is the reason we used a stiffness-based force control in contrast to direct force control.

Human–Robot Collaboration is a cogent need on the factory floors, particularly in the manufacturing and repair industries. In this paper, we presented a collaborative curve tracing technique targeting industrial tooling tasks, whereby the user physically interacts with the robot to engage in surface finishing tasks. We focused our study primarily on edge chamfering and polishing tasks, where, the tool trajectory can be represented analytically. By modulating impedance in parallel and orthogonal directions to the reference path, we imposed motion constraints on the combined human–robot motion.

Owing to the compliant feature of the robot (KUKA iiwa) and the geometrical properties of the surface, the user was able to generate the tool path, circumventing the necessity of programming expertise. The proposed framework was tested and validated by performing two sets of trials for both chamfering and polishing tasks. Each of the tasks was performed in a collaborative fashion with the robot operating as (a) a gravity compensator and (b) an assistant governed by the proposed impedance controlled curve tracing. In the context of the chamfering task, the resulting surface dimensions, as measured by a GapGun show that our approach yielded more consistent and accurate chamfer in comparison. As for the polishing task, from visual observation, we concluded that, employing the impedance controlled guidance results in a smooth finish, which is acceptable levels of defects arising from improper tool placement.

CRediT authorship contribution statement

Sreekanth Kana: Conceptualization, Methodology, Software, Writing, Verification. **Srinivasan Lakshminarayanan:** Conceptualization, Methodology, Software, Writing. **Dhanya Menoth Mohan:** Conceptualization, Methodology, Software, Writing. **Domenico Campolo:** Conceptualization, Methodology, Software, Writing, Funding acquisition.

Declaration of competing interest

The authors declare that they have no known competing financial interests or personal relationships that could have appeared to influence the work reported in this paper.

Acknowledgement

This project was conducted within the Rolls-Royce@NTU Corporate Lab with support from the National Research Foundation (NRF) Singapore under the Corp Lab@University Scheme.

References

[1] M. Amersdorfer, J. Kappey, T. Meurer, Real-time freeform surface and path tracking for force controlled robotic tooling applications, Robot. Comput.-Integr. Manuf. 65 (2020) 101955.

[2] J. Hong, D. Wang, Y. Guan, et al., Synergistic integrated design of an electrochemical mechanical polishing end-effector for robotic polishing applications, Robot. Comput.-Integr. Manuf. 55 (2019) 65–75.

[3] F. Nagata, Y. Kusumoto, Y. Fujimoto, K. Watanabe, Robotic sanding system for new designed furniture with free-formed surface, Robot. Comput.-Integr. Manuf. (ISSN: 07365845) 23 (4) (2007) 371–379.

[4] J.H. Ahn, Y.F. Shen, H.Y. Kim, H.D. Jeong, K.K. Cho, Development of a sensor information integrated expert system for optimizing die polishing, Robot. Comput.-Integr. Manuf. (ISSN: 07365845) 17 (4) (2001) 269–276.

[5] A.E.K. Mohammad, D. Wang, Electrochemical mechanical polishing technology: recent developments and future research and industrial needs, Int. J. Adv. Manuf. Technol. (ISSN: 14333015) 86 (5–8) (2016) 1909–1924.

[6] D.J. Buckmaster, W.S. Newman, S.D. Somes, Compliant motion control for robust robotic surface finishing, in: Proceedings of the World Congress on Intelligent Control and Automation, WCICA, 2008, pp. 559–564.

[7] J. Li, T. Zhang, X. Liu, Y. Guan, D. Wang, A survey of robotic polishing, in: 2018 IEEE International Conference on Robotics and Biomimetics, ROBIO 2018, IEEE, 2018, pp. 2125–2132.

[8] S. El Zaatari, M. Marei, W. Li, Z. Usman, Cobot programming for collaborative industrial tasks: An overview, Robot. Auton. Syst. (ISSN: 09218890) 116 (June) (2019) 162–180.

[9] F. Klocke, O. Dambon, B. Behrens, Analysis of defect mechanisms in polishing of tool steels, Prod. Eng. (ISSN: 09446524) 5 (5) (2011) 475–483.

[10] L. Peternel, W. Kim, J. Babič, A. Ajoudani, Towards ergonomic control of human-robot co-manipulation and handover, in: 2017 IEEE-RAS 17th International Conference on Humanoid Robotics, Humanoids, 2017, pp. 55–60, ISBN 2164-0580.

[11] E. Matheson, R. Minto, E.G.G. Zampieri, M. Faccio, G. Rosati, Human-robot collaboration in manufacturing applications: A review, Robotics (ISSN: 22186581) 8 (4) (2019) 1–25.

[12] A. Realyvásquez-Vargas, K.C. Arredondo-Soto, J.L. García-Alcaraz, B.Y. Márquez-Lobato, J. Cruz-García, Introduction and configuration of a collaborative robot in an assembly task as a means to decrease occupational risks and increase efficiency in a manufacturing company, Robot. Comput.-Integr. Manuf. 57 (2019) 315–328.

[13] D. Kragic, P. Marayong, M. Li, A.M. Okamura, G.D. Hager, Human-machine collaborative systems for microsurgical applications, Int. J. Robot. Res. (ISSN: 0278-3649) 24 (9) (2005) 731–741.

[14] N. Padoy, G.D. Hager, Human-machine collaborative surgery using learned models, in: Proceedings - IEEE International Conference on Robotics and Automation, IEEE, (ISSN: 10504729) 2011, pp. 5285–5292.

[15] K.R. Guerin, S.D. Riedel, J. Bohren, G.D. Hager, Adjutant: A framework for flexible human-machine collaborative systems, in: IEEE International Conference on Intelligent Robots and Systems, IEEE, (ISSN: 21530866) 2014, pp. 1392–1399.

[16] M. Tannous, M. Miraglia, F. Inglese, L. Giorgini, F. Ricciardi, R. Pelliccia, M. Milazzo, C. Stefanini, Haptic-based touch detection for collaborative robots in welding applications, Robot. Comput.-Integr. Manuf. 64 (2020) 101952.

[17] L. Johannsmeier, S. Haddadin, A hierarchical human-robot interaction-planning framework for task allocation in collaborative industrial assembly processes, IEEE Robot. Autom. Lett. (ISSN: 2377-3766) 2 (1) (2017) 41–48.

[18] E.I. Makrini, K. Merckaert, D. Lefeber, B. Vanderborght, Design of a collaborative architecture for human-robot assembly tasks, in: 2017 IEEE/RSJ International Conference on Intelligent Robots and Systems, IROS, pp. 1624–1629, 2017, ISBN: 2153-0866.

[19] N. Hogan, Impedance control: An approach to manipulation: Part III-applications, Trans. ASME, J. Dyn. Syst. Meas. Control (ISSN: 15289028) 107 (1) (1985) 17–24.

[20] C. Gaz, E. Magrini, A. De Luca, A model-based residual approach for human-robot collaboration during manual polishing operations, Mechatronics (ISSN: 09574158) 55 (2018) 234–247.

[21] L. Peternel, C. Fang, N. Tsagarakis, A. Ajoudani, A selective muscle fatigue management approach to ergonomic human-robot co-manipulation, Robot. Comput.-Integr. Manuf. 58 (2019) 69–79.

[22] S. Hamdan, E. Oztop, B. Ugurlu, Force reference extraction via human interaction for a robotic polishing task: force-induced motion, in: 2019 IEEE International Conference on Systems, Man and Cybernetics, SMC, IEEE, 2019, pp. 4019–4024.

[23] F. Pini, F. Leali, Human-robot collaborative reconfigurable platform for surface finishing processes, Procedia Manuf. 38 (2019) 76–83.

[24] L. Peternel, N. Tsagarakis, D. Caldwell, A. Ajoudani, Robot adaptation to human physical fatigue in human–robot co-manipulation, Auton. Robots 42 (5) (2018) 1011–1021.

[25] R.S. Jamisola, D.N. Oetomo, M.H. Ang, O. Khatib, T.M. Lim, S.Y. Lim, Compliant motion using a mobile manipulator: an operational space formulation approach to aircraft canopy polishing, Adv. Robot. 19 (5) (2005) 613–634.

[26] J.E. Solanes, L. Gracia, P. Muñoz-Benavent, J.V. Miro, V. Girbés, J. Tornero, Human-robot cooperation for robust surface treatment using non-conventional sliding mode control, ISA Trans. 80 (2018) 528–541.

[27] L.B. Rosenberg, Virtual fixtures: perceptual tools for telerobotic manipulation, in: 1993 IEEE Annual Virtual Reality International Symposium, 1993, pp. 76–82.

[28] L.B. Rosenberg, Virtual fixtures as tools to enhance operator performance in telepresence environments, in: Telemanipulator Technology and Space Telerobotics, vol. 2057, 1993, pp. 10–21.

[29] H.C. Lin, K. Mills, P. Kazanzides, G.D. Hager, P. Marayong, A.M. Okamura, R. Karam, Portability and applicability of virtual fixtures across medical and manufacturing tasks, in: Proceedings - IEEE International Conference on Robotics and Automation, vol. 2006, IEEE, (ISSN: 10504729) 2006, pp. 225–230.

[30] L.B. Rosenberg, Virtual haptic overlays enhance performance in telepresence tasks, in: Telemanipulator and Telepresence Technologies, vol. 2351, 1995, pp. 99–108.

[31] A. Bettini, P. Marayong, S. Lang, A.M. Okamura, G.D. Hager, Vision-assisted control for manipulation using virtual fixtures, IEEE Trans. Robot. (ISSN: 15523098) 20 (6) (2004) 953–966.

[32] K. Sreekanth, D.M. Mohan, H. Bo, D. Campolo, Manual guidance of a compliant manipulator during curve-following tasks: Basic framework and preliminary experimental tests, in: IEEE Region 10 Annual International Conference, Proceedings/TENCON, ISBN: 9781509025961, 2017.

[33] M.D. Carmo, Differential Geometry of Curves and Surfaces: Revised and Updated Second Edition, 2016.

[34] F. Ficuciello, L. Villani, B. Siciliano, Variable impedance control of redundant manipulators for intuitive human–robot physical interaction, IEEE Trans. Robot. 31 (4) (2015) 850–863.

[35] C. Ott, R. Mukherjee, Y. Nakamura, Unified impedance and admittance control, in: 2010 IEEE International Conference on Robotics and Automation, IEEE, 2010, pp. 554–561.

[36] K.P. Tee, E. Burdet, C.-M. Chew, T.E. Milner, A model of force and impedance in human arm movements, Biol. Cybernet. 90 (5) (2004) 368–375.

[37] S. Kana, K.-P. Tee, D. Campolo, Human–robot co-manipulation during surface tooling: A general framework based on impedance control, haptic rendering and discrete geometry, Robot. Comput.-Integr. Manuf. 67 (2021) 102033.

[38] S. Lakshminarayanan, S. Kana, D.M. Mohan, O.M. Manyar, D. Then, D. Campolo, An adaptive framework for robotic polishing based on impedance control, Int. J. Adv. Manuf. Technol. (2020) 1–17.